A QCL Model with Integrated Thermal and Stark Rollover Mechanisms

Gary Agnew, *Member, IEEE,* Andrew Grier, Thomas Taimre, *Associate Member, IEEE,* Yah Leng Lim, Zoran Ikonić, Paul Dean, Suraj P. Khanna, Mohammad Lachab, Alexander Valavanis, Jonathan Cooper, Paul Harrison, Edmund H. Linfield, A. Giles Davies, Dragan Indjin, and Aleksandar D. Rakić, *Senior Member, IEEE*

***Abstract*—There is a need for a model that accurately describes dynamics of a bound-to-continuum terahertz quantum cascade laser over its full range of operating temperatures and bias conditions. In this paper we propose a compact model which, through the inclusion of thermal and Stark effects, accurately reproduces the light-current characteristics of an exemplar bound-to-continuum terahertz quantum cascade laser. Through this model, we investigate the dynamics of this laser with a view to applications in high-speed free space communications.**

***Index Terms*—Free space communication, quantum cascade laser, rate equation, Stark effect, thermal rollover**

I. Introduction

Current practice in quantum cascade laser (QCL) rate equation (RE) modeling focuses on device behavior over a relatively narrow temperature and voltage range by using reduced RE parameters having fixed values; that is, independent of temperature and voltage [1], [2], [3]. While this approach may suffice for some research and design activities, there remains a need for a more flexible and complete model. Such a model would ideally be capable of efficiently (in the computational sense) and accurately capturing the static and dynamic behavior of the device over the full limits of its temperature and voltage operating ranges. In this paper we introduce a new reduced RE model that for the first time addresses and, we believe, meets these needs.

The development of our model has two main parts, both discussed in more detail in Section II. The first part is the determination of a behavioral model for each RE parameter from first principles, using a Schrödinger–Poisson (SP) self-consistent scattering transport solver [4], [5]. This is achieved by solving the SP equations for the complete structure at a number of temperatures and voltages, and then fitting a polynomial function to the resulting data for each RE parameter in our reduced REs. The "complete structure" in this context means rate equations for all states present in each period, as opposed to the reduced RE system used in the second part of our work. This process yields a set of polynomials that are functions of both temperature and voltage for use with the reduced REs.

The second part is the development of our novel REs. In a departure from conventional three-level RE practice, we introduce a differential equation that models the thermal behavior of the laser chip. This thermal equation solves for the device lattice temperature which is subject to change as a result of self-heating and ambient temperature changes — but more importantly, provides a dynamic temperature input for the temperature-dependent RE parameter polynomials. The terminal voltage of the device together with the lattice temperature allows all of the RE parameters to be calculated from their (behavioral) polynomials, thereby producing accurate solutions to the REs over a broad range of voltages and temperatures.

An additional departure from conventional practice is our use of RE parameters that are functions of both temperature and voltage. It is this feature that gives our model the ability to capture both the static and dynamic behavior of the device over its full voltage and temperature operating range. Further, we make provision for gain compression and injection of carriers into both the upper and lower lasing levels, subsequently referred to as ULL and LLL, respectively.

Section III presents the results of some static and dynamic simulations applied to an exemplar bound-to-continuum terahertz (THz) QCL [6], as an illustration of how device behavior changes with temperature and voltage.

II. Modeling Method

A. Exemplar device

The device we chose to model is a GaAs/AlGaAs Fabry–Pérot, single-mode, 90 period, bound-to-continuum THz QCL emitting at 2.59 THz. More information about the structure of this device can be found in [7]. The device was designed to operate at temperatures under 50 K in continuous wave mode, and thus requires cryostatic operation.

B. RE parameter behavioral modeling

A thermally-balanced self-consistent SP RE scattering transport model [8], [5] for all states in the device was applied in a grid of 13 temperatures and 38 electric field values (voltages). From these calculations we extracted values for

G. Agnew, Y. L. Lim, and A. D. Rakić are with the School of Information Technology and Electrical Engineering, The University of Queensland, Brisbane, Queensland, 4072, Australia (corresponding author can be reached at phone: +61-7-3365-8301; fax: +61-7-3365-4999; e-mail: g.agnew@uq.edu.au).

T. Taimre is with the School of Mathematics and Physics, The University of Queensland, Brisbane, Queensland, 4072, Australia

A. Grier, D. Indjin, Z. Ikonić, P. Dean, S. Khanna, M. Lachab, A. Valavanis, J. Cooper, E. Linfield, and A. Davies are with the School of Electronic and Electrical Engineering, University of Leeds, Leeds LS2 9JT, U.K.

P. Harrison is with the Materials and Engineering Research Institute, Sheffield Hallam University, Sheffield, S1 1WB, United Kingdom

the reduced RE parameters: gain factor, upper and lower laser level lifetimes, injection efficiencies into these levels, as well as the scattering time between them, giving a total of 494 grid point values for each RE parameter. Hybridized wave functions of electron states occur commonly and somewhat unpredictably in the process of solving the SP equations [9], resulting in non-physical RE parameters being produced. All such non-physical parameters have to be removed from the data set.

Finally, a third order polynomial in two variables (voltage V and temperature T) was fitted to the remaining data for each parameter using a least-squares method, giving a simple and smooth function for use in the REs.

C. Rate equation model

Our set of four REs reads:

$$\frac{\mathrm{d}S(t)}{\mathrm{d}t} = -\frac{1}{\tau_\mathrm{p}} S(t) + \frac{\beta_\mathrm{sp}}{\tau_\mathrm{sp}(T,V)} N_3(t) + MG(T,V)\frac{(N_3(t)-N_2(t))}{1+\varepsilon S(t)} S(t) \quad (1)$$

$$\frac{\mathrm{d}N_3(t)}{\mathrm{d}t} = -G(T,V)\frac{(N_3(t)-N_2(t))}{1+\varepsilon S(t)} S(t) - \frac{1}{\tau_3(T,V)} N_3(t) + \frac{\eta_3(T,V)}{q} I(t) \quad (2)$$

$$\frac{\mathrm{d}N_2(t)}{\mathrm{d}t} = +G(T,V)\frac{(N_3(t)-N_2(t))}{1+\varepsilon S(t)} S(t) + \frac{1}{\tau_{32}(T,V)} N_3(t) + \frac{\eta_2(T,V)}{q} I(t) - \frac{1}{\tau_{21}(T,V)} N_2(t) \quad (3)$$

$$\frac{\mathrm{d}T(t)}{\mathrm{d}t} = \frac{1}{mc}\left(I(t)V(T(t),I(t)) - \frac{(T(t)-T_0)}{R_\mathrm{th}} \right) \quad (4)$$

The symbol $S(t)$ represents the photon population, τ_p the photon lifetime in the cavity, $N_3(t)$ the ULL carrier number, $N_2(t)$ the LLL carrier number, $I(t)$ the current forcing function, q the electronic charge, β_sp the spontaneous emission factor, τ_sp the spontaneous emission lifetime (or radiative spontaneous relaxation time), and M is the number of periods in the structure, 90 in the case of our exemplar device. The η_3 term in (2) models carrier injection efficiency into the ULL and the η_2 term in (3) models carrier injection efficiency directly into the LLL. The carrier lifetime for non-radiative transitions from the ULL to LLL is τ_{32}, the total lifetime due to non-radiative transitions for the ULL carrier population is τ_3, and the lifetime for transitions from the LLL to the continuum is τ_{21}. The gain factor is represented by G, as defined in [3]. We make provision for gain compression by including the term in ε in (1) to (3).

To model thermal transients caused by self-heating and changes in ambient temperature, our REs include (4), a differential equation for the lattice temperature of the laser. This equation models the first order thermal behavior of the device, and produces dynamic temperature data required to determine the temperature-sensitive RE parameters. In (4), m represents the effective mass of the laser in kg, c the effective specific heat capacity of the laser material in J kg^{-1} K^{-1} and R_th the effective thermal resistance in K W^{-1} between the laser chip and its mount, in this case the cold finger of the cryostat. The symbol T_0 is the temperature (in K) of the cold finger which is usually (but not necessarily) constant.

The voltage V at the device terminals, expressed as $V(T(t), I(t))$ in (4), was modeled by fitting a third order polynomial in two variables (current I and temperature T) to the experimentally determined current-voltage (IV) characteristics of the device, having been measured over a range of currents and temperatures. The voltage V may then be determined from the third order polynomial model at any given current and temperature. The voltage thus determined is then used to calculate all other parameters that depend on it.

RE parameters that depend on voltage (V) and temperature (T) are expressed as functions of V and T in the REs. These include the gain factor G, injection efficiencies η_3 and η_2, and carrier lifetimes τ_3, τ_{32}, and τ_{21}. The voltage V and temperature T are themselves time-dependent, but for the sake of readability are not written explicitly as functions of time t in (1) to (3).

Initial values for carrier and photon populations, the current forcing function $I(t)$, and T_0, serve as independent inputs to the REs (1) to (4). Given the inputs and the RE parameters as functions of V and T as described in Section II.B, the REs may be solved for carrier and photon population. The optical output power P can then be found from the photon population using the following relation [2]:

$$P(t) = \eta_0 \hbar \omega S(t)/\tau_\mathrm{p}\,, \quad (5)$$

where η_0 is the power output coupling efficiency [2], $\hbar$ is the reduced Planck constant, and ω is the laser's angular emission frequency.

III. Results and Discussion

After determining behavioral models for our exemplar device, MATLAB's (MathWorks, Inc.) `ode23s` solver was used to find carrier and photon populations, temperature, and optical output power for two current forcing functions and cold finger temperatures.

The first forcing function, chosen to illustrate our model's ability to capture the salient features of the device's light-current (LI) curves, is a slow, linear, one-second current sweep from 300 mA to 700 mA. A low speed current sweep is used to ensure the simulated light output is for truly static conditions, and is not affected by thermal transients. This stimulus, when used with the conventional three-level rate equations (having fixed parameters), produces an LI curve that is a straight line ascending from the threshold current, as illustrated in [2]. Figure 1 shows our LI solutions for three cold finger temperatures. For comparison, Fig. 2 shows the device's measured LI curves at the same cold finger temperatures. The steep decline in light output above 500 mA is due to

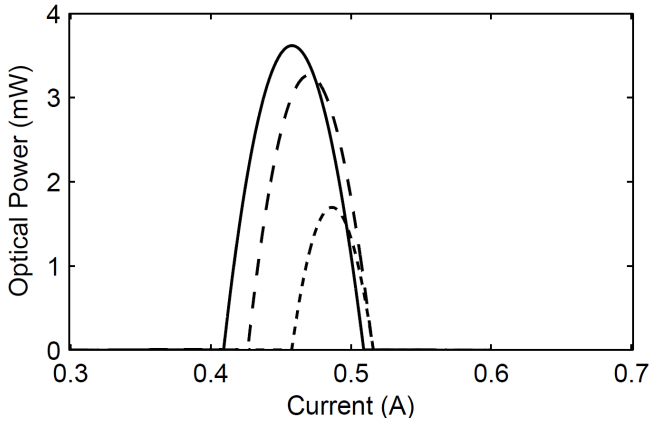

Fig. 1. Simulated LI response of QCL at three cold finger temperatures. The solid line is for a cold finger temperature of 10 K, the broken line for 20 K, and the dotted line for 40 K.

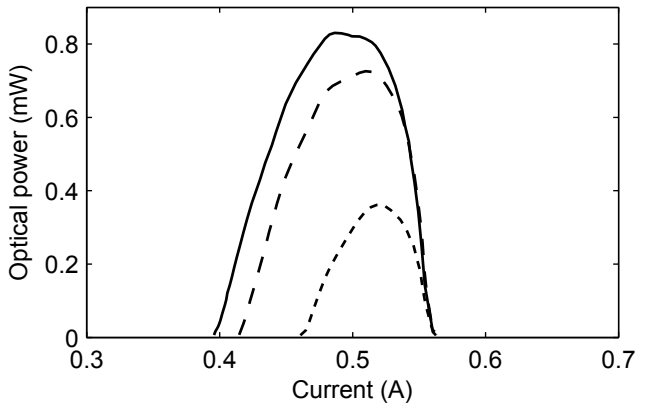

Fig. 2. Measured LI response of QCL at three cold finger temperatures. The solid line is for a cold finger temperature of 10 K, the broken line for 20 K, and the dotted line for 40 K.

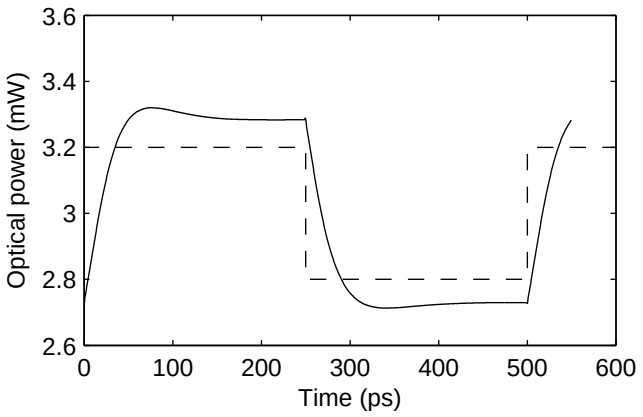

Fig. 3. Solid line: transient response to square wave modulation of peak-to-peak amplitude 10mA (broken line) with a bias offset of 441 mA (in ascending part of LI curve) and cold finger temperature 10 K . The broken line indicates timing of the current pulses only.

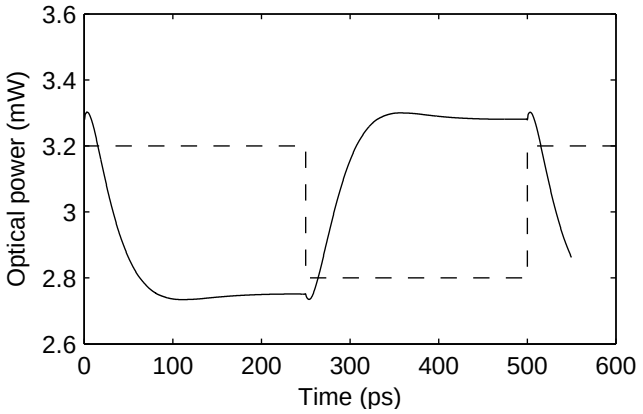

Fig. 4. Solid line: transient response to square wave modulation of peak-to-peak amplitude 10 mA with a bias offset of 475 mA (in descending part of LI curve) and cold finger temperature 10 K. The broken line indicates timing of the current pulses only.

the Stark effect [10], [11], a phenomenon that is captured by our model and is manifested in the RE parameters as a sharp drop in injection efficiency with rising terminal voltage. The use of a third-order polynomial function to model η_3 leads to values slightly lower than correct near the threshold and cutoff currents, and slightly higher than correct midway through the curve, giving rise to the more peaked appearance of the simulated curves. The disagreement in the maxima (around 0.8 mW in the measured results as opposed to 3.5 mW in the simulation) are due to the poor collection efficiency of the measurement device.

The second current forcing function was chosen to illustrate the ability of our model to capture high speed device dynamics and show how the dynamics change with bias (operating point). A square current waveform of period 500 ps and peak-to-peak amplitude 10 mA was superimposed with a DC (bias) current of two values: one at 441 mA (the rising part of the LI curve in Fig. 1) and the other at 475 mA (the falling part of the LI curve in the same figure). The transient response for the 441 mA bias shown in Fig. 3 and the transient response for the 475 mA bias is shown in Fig. 4.

We note that in addition to the inversion, there are clearly distinguishable differences in the waveform at the two bias points. In free space communications applications [12], [13], [14], [15], the most important difference would be in the rise times of the responses which are, respectively, 50 ps and 81 ps (using the 0%–100% definition of rise time). Although the rising edge in Fig. 4 corresponds to a falling one in Fig. 3, the "rise" and "fall" (transition) times in each figure are the same due to the symmetry of the waveforms. The differing transition times indicate that in such an application, a higher bandwidth (data throughput rate) would be attainable at the lower bias point. On the other hand, the temperature stability of the higher bias point is far better. In an environment in which a QCL's heat sink temperature is not well controlled, it could be advantageous to operate at the higher bias point with better temperature stability, at the expense of some bandwidth loss. Such a scenario could arise in applications in the near future, using THz QCLs capable of operating efficiently at Peltier cooler temperatures. We note further that transient responses lack relaxation oscillations, corroborating the findings of others [16], [17].

IV. Conclusion

Initial results suggest that our modeling approach may be useful for exploring and characterizing THz QCL behavior. The novelty of our approach is the use of RE parameters that are functions of device voltage and lattice temperature, and are derived from first principles by the SP approach. Coupled with a time dependent thermal equation, behavioral modeling of RE parameters in this way gives a RE model that is valid over a very broad range of device temperatures and voltages, and allows for a seamless exploration of the device's characteristics.

Our illustrative examples of both steady state and dynamic solutions have shown the simulations to compare very well with measurements and well-known characteristics of the exemplar bound-to-continuum THz QCL.

Acknowledgments

This research was supported under Australian Research Councils Discovery Projects funding scheme (DP 120 103703). We also acknowledge support of the ERC NOTES and TOSCA programmes, the Royal Society, the Wolfson Foundation, and the European Cooperation in Science and Technology (COST) Action BM1205. Y.L.L. acknowledges support under the Queensland Governments Smart Futures Fellowships programme. G.A. acknowledges the support of an Australian Postgraduate Award (APA). P.D. acknowledges support from the EPSRC (UK).

References

[1] A. Hamadou, S. Lamari, and J. L. Thobel, "Dynamic modeling of a midinfrared quantum cascade laser," *J. Appl. Phys.*, vol. 105, no. 9, pp. 1–6, 2009.

[2] A. Hamadou, J. L. Thobel, and S. Lamari, "Modelling of temperature effects on the characteristics of mid-infrared quantum cascade lasers," *Opt. Commun.*, vol. 281, no. 21, pp. 5385–5388, 2008.

[3] Y. Petitjean, F. Destic, J. C. Mollier, and C. Sirtori, "Dynamic modeling of terahertz quantum cascade lasers," *IEEE J. Sel. Top. Quant. Electron.*, vol. 17, no. 1, pp. 22–29, 2011.

[4] V. D. Jovanović, D. Indjin, N. Vukmirović, Z. Ikonić, P. Harrison, E. H. Linfield, H. Page, X. Marcadet, C. Sirtori, C. Worrall, H. E. Beere, and D. A. Ritchie, "Mechanisms of dynamic range limitations in GaAs/AlGaAs quantum-cascade lasers: Influence of injector doping," *Appl. Phys. Lett.*, vol. 86, no. 21, pp. 1–3, 2005.

[5] V. D. Jovanović, S. Höfling, D. Indjin, N. Vukmirović, Z. Ikonić, P. Harrison, J. P. Reithmaier, and A. Forchel, "Influence of doping density on electron dynamics in GaAs/AlGaAs quantum cascade lasers," *J. Appl. Phys.*, vol. 99, no. 10, 2006.

[6] S. Barbieri, J. Alton, H. E. Beere, J. Fowler, E. H. Linfield, and D. A. Ritchie, "2.9 THz quantum cascade lasers operating up to 70 K in continuous wave," *Appl. Phys. Lett.*, vol. 85, no. 10, pp. 1674–1676, 2004.

[7] A. D. Rakić, T. Taimre, K. Bertling, Y. L. Lim, P. Dean, D. Indjin, Z. Ikonić, P. Harrison, A. Valavanis, S. P. Khanna, M. Lachab, S. J. Wilson, E. H. Linfield, and A. G. Davies, "Swept-frequency feedback interferometry using terahertz frequency QCLs: A method for imaging and materials analysis," *Opt. Express*, vol. 21, no. 19, pp. 22 194–22 205, 2013.

[8] D. Indjin, P. Harrison, R. W. Kelsall, and Z. Ikonic, "Self-consistent scattering theory of transport and output characteristics of quantum cascade lasers," *J. Appl. Phys.*, vol. 91, no. 11, 2002.

[9] H. Callebaut and Q. Hu, "Importance of coherence for electron transport in terahertz quantum cascade lasers," *J. Appl. Phys.*, vol. 98, no. 10, 2005.

[10] S. S. Howard, Z. Liu, and C. F. Gmachl, "Thermal and stark-effect roll-over of quantum-cascade lasers," *IEEE J. Quant. Electron.*, vol. 44, no. 4, pp. 319–323, 2008.

[11] S. S. Howard, Z. Liu, and C. Gmachl, "Analysis of the thermal roll-over of quantum cascade lasers," in *CLEO, Conference on Lasers and Electro-Optics*, 2007.

[12] S. Barbieri, W. Maineult, S. S. Dhillon, C. Sirtori, J. Alton, N. Breuil, H. E. Beere, and D. A. Ritchie, "13 GHz direct modulation of terahertz quantum cascade lasers," *Appl. Phys. Lett.*, vol. 91, no. 14, 2007.

[13] R. Martini, C. Bethea, F. Capasso, C. Gmachl, R. Paiella, E. A. Whittaker, H. Y. Hwang, D. L. Sivco, J. N. Baillargeon, and A. Y. Cho, "Free-space optical transmission of multimedia satellite data streams using mid-infrared quantum cascade lasers," *Electron. Lett.*, vol. 38, no. 4, pp. 181–183, 2002.

[14] R. Martini, C. Gmachl, R. Paiella, F. Capasso, C. Glazowski, R. Murawski, E. A. Whittaker, C. G. Bethea, H. Y. Hwang, D. L. Sivco, J. N. Baillargeon, A. Y. Cho, and H. C. Liu, "Analog and digital high-speed modulation of quantum-cascade laser," in *Proc. SPIE-Int. Soc. Opt. Eng.*, vol. 4995, 2003, pp. 169–175.

[15] R. Martini and E. A. Whittaker, "Quantum cascade laser-based free space optical communications," *J. Opt. Fiber. Commun. Rep.*, vol. 2, no. 4, pp. 279–292, 2005.

[16] R. Martini, R. Paiella, F. Capasso, C. Gmachl, H. Y. Hwang, D. L. Sivco, A. Y. Cho, E. A. Whittaker, and H. C. Liu, "Absence of relaxation oscillation in quantum cascade lasers verified by high-frequency modulation," in *CLEO Europe - Technical Digest*, 2001, pp. CPD17–1–CPD17–2.

[17] R. Paiella, R. Martini, F. Capasso, C. Gmachl, H. Y. Hwang, D. L. Sivco, J. N. Baillargeon, A. Y. Cho, E. A. Whittaker, and H. C. Liu, "High-frequency modulation without the relaxation oscillation resonance in quantum cascade lasers," *Appl. Phys. Lett.*, vol. 79, no. 16, pp. 2526–2528, 2001.